

One step synthesis of $\text{Fe}_{4.4}\text{Ni}_{17.6}\text{Se}_{16}$ coupled NiSe foam as self-supported, highly efficient and durable oxygen evolution electrode

Sainan Ma^{1,2}, Huiyu yuan^{1,2}, Lejuan Cai², Xinyu Wang^{1,2}, Hui Long^{1,2}, Yang Chai², Yuen Hong Tsang^{1,2*}

¹ The Hong Kong Polytechnic University Shenzhen Research Institute, Shenzhen, People's Republic of China

² Department of Applied Physics and Materials Research Center, The Hong Kong Polytechnic University, Hung Hom, Kowloon, Hong Kong, People's Republic of China

E-mail: yuen.tsang@polyu.edu.hk

Keywords: electrocatalyst, $\text{Fe}_{4.4}\text{Ni}_{17.6}\text{Se}_{16}$ /NiSe hybrid, heterointerfaces, oxygen evolution reaction, thermal selenization

Abstract

The development of cost-effective, durable and high-efficient oxygen evolution reaction (OER) electrocatalysts is an extremely critical technology for the large-scale industrial water electrolysis. Here, a new strategy is proposed to significantly enhance the electrocatalytic activity by forming a hybrid electrode of NiSe and $\text{Fe}_{4.4}\text{Ni}_{17.6}\text{Se}_{16}$ through direct selenization of porous iron-nickel (FeNi) alloy foam via thermal selenization process. The obtained self-supported $\text{Fe}_{4.4}\text{Ni}_{17.6}\text{Se}_{16}$ /NiSe hybrid (FNS/NiSe) foam displays outstanding durability and remarkable catalytic activity in 1.0 M KOH with low overpotentials of 242 and 282 mV to achieve the current densities of 100 and 500 mA cm^{-2} , respectively. To the best of our knowledge, it exceeds most of the reported OER electrocatalysts in alkaline electrolytes.

1. Introduction

The excessive consumption of fossil fuels and increasing climate issues have made it critical to develop green, sustainable and renewable energy sources [1,2]. Electrochemical water splitting arises to be a highly promising strategy to mass-produce hydrogen and oxygen, in which oxygen evolution reaction (OER; $4\text{OH}^- \rightarrow \text{O}_2 + 2\text{H}_2\text{O} + 4\text{e}^-$) is an important half-reaction [3,4]. However, OER is a complex and kinetically sluggish process involving multistep proton-coupled electron transfer process with a high overpotential [5]. Consequently, effective electrocatalysts are essential for accelerating the reaction rate and reduce energy loss. Nowadays, the precious metal-based catalysts such as RuO_2 and IrO_2 play an active role in OER, but these materials are scarce and highly cost, which limits their large-scale practical applications in industry [6]. Over the past few decades, numerous efforts have been devoted to search for highly efficient, durable and cost-effective materials as alternatives.

Recently, nonprecious first-row transition metals, especially Fe, Ni and Co, have attracted extensive attentions due to their earth-abundant nature and rich variable compositions (metal hydroxides, phosphides, sulfides and selenide, etc.) [7-9]. Among them, nickel selenides, such as NiSe , NiSe_2 , and Ni_3Se_2 , are found to exhibit appreciable electrocatalytic performance for water splitting [10-15]. For instance, Nath et al. electrodeposited Ni_3Se_2 films on the Au-coated Si substrate with an overpotential of 290 mV to reach a current density of 10 mA cm^{-2} towards OER [13]. Sun and co-workers synthesized NiSe nanowire film *in situ* on Ni foam by hydrothermal method as an efficient OER electrode, which demonstrates an overpotential of 270 mV to drive a current density of 20 mA cm^{-2} [14]. However, achieving lower overpotential is still a big challenge for these nickel selenides due to the limited electronic conductivity and stability [16]. It has been reported that utilization of hybrid materials can improve the charge transfer and exhibit higher electrocatalytic performance due to the strong coupling and synergetic effects of the polyphaser catalysts [17-20]. For example, Li *et al.* developed hybrids

NiSe₂/Fe₃Se₄/C nanorods derived from Ni/Fe metal-organic frameworks, in which Ni and Fe sites collaborate well with each other and realize a low overpotential of 240 mV under a current density of 10 mA cm⁻² [21]. Shen's group reported a eutectic NiSe/Ni₃Se₂ electrocatalyst grown on Ni foam with remarkable electrochemical activities, in which interface reconstruction between NiSe and Ni₃Se₂ leads to the re-distribution of charge and thus reduces the energy barrier [22]. Design and fabrication of high quality selenides-based hybrid catalysts is obviously a viable approach to enhance the catalysis performance. However, despite these progress, the relatively complex synthetic methods with complicated recipes still hinder the development of hybrid electrocatalysts for OER.

Here, in our work, we report a Fe_{4.4}Ni_{17.6}Se₁₆/NiSe hybrid foam (denoted as FNS/NiSe foam) achieved via a one-step thermal selenization process by direct selenization of FeNi alloy foam as self-supported OER electrode. Selenization of FeNi foams under 550 °C can produce the integrated FNS/NiSe foam, which exhibits superior electrochemical activity and durability for OER, with an exceptional overpotential of 242 mV to deliver a current density of 100 mA cm⁻² in 1.0 M KOH.

2. Material and methods

2.1. Materials

FeNi alloy foam (Fe/Ni, 1:3.8) and Ni foam were purchased from Jiangsu Jiayisheng Metal Materials Co., Ltd. Acetic acid (99.8%) and KOH (cat. no. P5958) were purchased from Sigma-Aldrich Chemical Reagent Co., Ltd. Ethanol with ACS grade was bought from the Anaqua Global International Inc., Ltd. Nafion (5 wt%) and Selenium powder (-325 mesh, 99.5%) was purchased from Alfa Aesar. Polyvinyl pyrrolidone (PVP, K30) was purchased from Sinopharm Chemical Reagent Co., Ltd. All the received chemicals were used without further purification. The deionized water used throughout all experiments was from a Millipore system.

2.2. Preparation of FNS/NiSe, FNS and NiSe foam

The Commercially purchased FeNi alloy foam and Ni foam were cut into pieces with an area of $1 \times 2 \text{ cm}^2$, which were washed under sonication by ethanol and DI water for 20 min to be well cleaned. After drying by N_2 gas, the cleaned FeNi foam was immersed into the PVP/HAc solution consisting of 0.1 g PVP in 5 ml HAc for several seconds and dried naturally [23]. PVP solution treatment was applied to increase the surface roughness according to a previously published study [23]. Then the freshly PVP/HAc treated FeNi foam and 250 mg of Se powder were placed in a quartz boat with Se powder at the upstream side of the tube furnace, followed by annealing at 550°C for 1 h with a heating rate of 5°C min^{-1} under argon atmosphere, and finally cooled to ambient temperature naturally to obtain the FNS/NiSe foam. The FNS foam was synthesized under the same procedure except for a higher annealing temperature of 650°C . For comparison, NiSe foam was also prepared under the same procedure except for using the Ni foam as the precursor under a temperature of 550°C .

2.3. Characterization

SEM images were obtained on a field-emission scanning electron microscope (JSM-6490, JEOL) operated at an accelerating voltage of 5 kV. XRD data were collected on an X-ray diffractometer (Rigaku SmartLab) using $\text{Cu K}\alpha$ ($\lambda = 1.54178 \text{ \AA}$) radiation. TEM images, HRTEM images and elemental mappings were acquired on a JEOL model JEM-2100F microscope. X-ray photoelectron spectroscopy (XPS) was performed on an ESCALAB 250Xi XPS instrument using Mg as the excitation source.

2.4. Electrochemical measurements

Electrochemical measurements were performed with a CHI 660E electrochemical workstation (Shanghai Chenhua Limited, China) in a standard three-electrode system at room temperature. An aqueous solution of 1.0 M KOH ($\text{pH} = 14$) was used as the electrolyte. The fabricated catalysts were used as working electrode without further treatments. A graphite rod and Hg/HgO (1.0 M NaOH) were used as the counter electrode and reference electrode, respectively. All potentials measured in our test were calibrated to reversible hydrogen

electrode according to the following equation: $E(\text{RHE}) = E(\text{Hg/HgO}) + 0.098 + 0.059 \text{ pH}$. The linear sweep voltammetry (LSV) measurements were recorded at a scan rate of 1.0 mV s^{-1} . All the LSV curves were 95% iR corrected by the IR compensation function on the CHI 660E electrochemical workstation [24]. Before test, catalysts were all activated by a chronopotentiometry scan with a constant current of 10 mA cm^{-2} to a stable state. The electrochemical double-layer capacitance (C_{dl}) was performed to determine the electrochemically active surface area (ECSA) from the scan-rate dependence of CVs. The scan rate increased from 5 mV s^{-1} to 60 mV s^{-1} with a 5 mV s^{-1} interval. The double-layer capacitance (C_{dl}) was then estimated by plotting the $\Delta J = (J_a - J_c)$ at a certain potential against the scan rate. The C_{dl} was half of the value of the linear slope. Electrochemical impedance spectroscopy (EIS) experiments were conducted in Solartron Electrochemical workstation (German) with the frequency ranging from 0.01 to 10^5 Hz at small AC voltage amplitude in 1.0 M KOH. Cyclic voltammetry (CV) and chronopotentiometry measurements were recorded under the same experimental setup without iR correction to evaluate the long-term stability.

3. Results and discussion

3.1. Catalyst structure, morphology and composition

The original FeNi alloy foam and Ni foam was firstly characterized by XRD. The XRD pattern of the FeNi alloy foam (Fig. S1 in the Supporting Information) is in good accordance with previous XRD pattern of FeNi alloy [25,26]. Fig. 1a presents the XRD patterns of the synthesized samples. The XRD pattern of the FNS/NiSe foam shows the characteristic peaks at 32.69° , 33.20° , 43.95° , 49.73° , 58.89° , 60.85° , 68.68° and 69.36° corresponding to the (101), (002), (102), (110), (103), (201), (202) and (004) planes of NiSe (JCPDS No. 65-6014), respectively; and the other peaks in the XRD pattern at 29.29° , 35.28° , 38.74° , 47.85° , 54.58° can be indexed to $\text{Fe}_{4.4}\text{Ni}_{17.6}\text{Se}_{16}$ (JCPDS No. 71-2282), respectively. The XRD patterns of the NiSe foam and FNS foam identify solely NiSe and $\text{Fe}_{4.4}\text{Ni}_{17.6}\text{Se}_{16}$, respectively, in these films.

It is noted that no peaks corresponding to NiFe or Ni foam were detected after selenization, indicating the complete selenization in all the samples. The typical morphologies of the original FeNi alloy foam and the as-obtained FNS/NiSe foam were shown in Fig. 1b and 1d. The FNS/NiSe foam retains the 3D cross-linked skeleton of FeNi alloy foam, which is expected to allow the efficient contact between catalysts and electrolyte and facilitate the easy release of generated O₂ gas during OER activity. Fig. 1c and 1e show the SEM images of the surfaces of the FeNi alloy and FNS/NiSe foams at higher magnifications, respectively. Obviously, the foam surface exhibits a highly stacked platelike structure after the selenization process, which is significantly different from the original FeNi alloy foam.

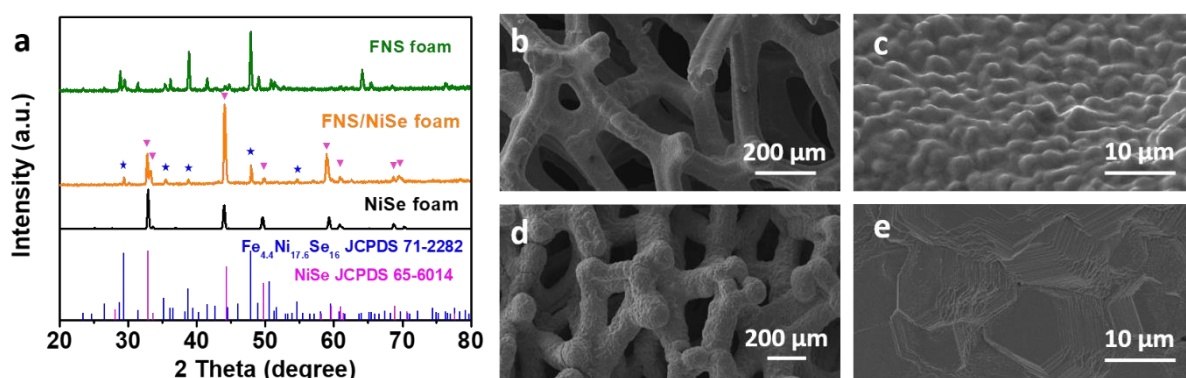


Fig. 1. (a) XRD patterns of the as-synthesized FNS foam, FNS/NiSe foam and NiSe foam. SEM images of (b, c) and (d, e) FNS/NiSe foam in different magnifications.

Fig. 2a shows the TEM image of the FNS/NiSe composites carefully scraped off from the FNS/NiSe foam. In the high-resolution TEM (HRTEM) shown in Fig. 2b, the lattice fringes with a lattice distance of 0.206 nm can be indexed to the (102) plane of NiSe, while the lattice fringes with a lattice distance of 0.187 nm matches with the (224) plane of Fe_{4.4}Ni_{17.6}Se₁₆. As displayed in Fig. 2b, a clear heterostructural interface is constituted by the (102) plane of NiSe and the neighbouring (224) plane of Fe_{4.4}Ni_{17.6}Se₁₆ (as indicated by the white dashed line), which is frequently found in our HRTEM data. Fig. 2c shows the TEM and EDX elemental mapping images. It is clear that the Fe, Ni and Se elements are homogeneously distributed in

the sample, providing a strong evidence for the uniform distribution of $\text{Fe}_{4.4}\text{Ni}_{17.6}\text{Se}_{16}$ in the main phase of NiSe. All results confirm the successful selenization of the FeNi alloy foam.

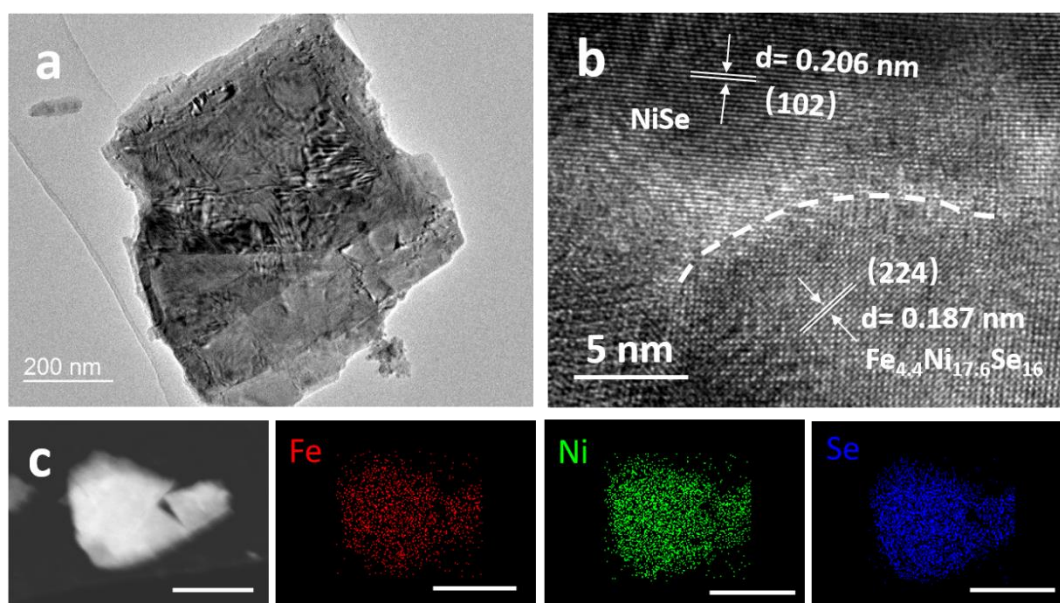


Fig. 2. (a) TEM and (b) corresponding HRTEM images of the FNS/NiSe composites. (c) The bright filed TEM image and EDX elemental mappings of Fe, Ni and Se for the FNS/NiSe composites (Scale bar: 300 μm).

X-ray photoelectron microscopy (XPS) was further conducted to investigate the elemental composition of the FNS/NiSe foam. All the binding energies were calibrated to C1s graphitic peak (284.6 eV). Fig. 3a shows the XPS spectrum of Ni 2p with two spin-orbit doublets and two satellite peaks. The peaks at 852.36, 855.42, 869.38 eV and 873.36 eV corresponding to Ni^{2+} 2p_{3/2}, Ni^{3+} 2p_{3/2}, Ni^{2+} 2p_{1/2} and Ni^{3+} 2p_{1/2}, respectively, can be associated with nickel selenides and oxidized nickel [27,28]. The Fe 2p XPS spectrum in Fig. 3b shows that, the binding energy peaks at 710.02 eV and 723.93 eV are attributed to Fe^{2+} 2p_{3/2} and Fe^{2+} 2p_{1/2}, respectively; The peaks at 711.66 eV and 726.81 eV correspond to Fe^{3+} 2p_{3/2} and Fe^{3+} 2p_{1/2}, respectively. These binding energy peaks can be assigned to iron selenide and iron oxides [21,24]. The XPS spectrum of Se 3d in Fig. 3c shows the characteristic peaks of the Se 3d binding energy at 54.56 and 56.41 eV, indicating the formation of selenide species binding with

the Fe and Ni irons [29,30]. These results suggest the successful selenization of FeNi alloy foam into metal selenides, which is consistent with the aforementioned XRD results. In addition, the XPS characterization of NiSe foam were also carried out for comparison. As displayed in Fig. 3d, the peak for Ni^{2+} 2p_{3/2} in FNS/NiSe foam exhibits a shift of about 0.4 eV compared to that of NiSe foam, which is supposed due to the construction of heterointerfaces in the FNS/NiSe foam. The binding energy shift has been found in several hybrid systems [20,28].

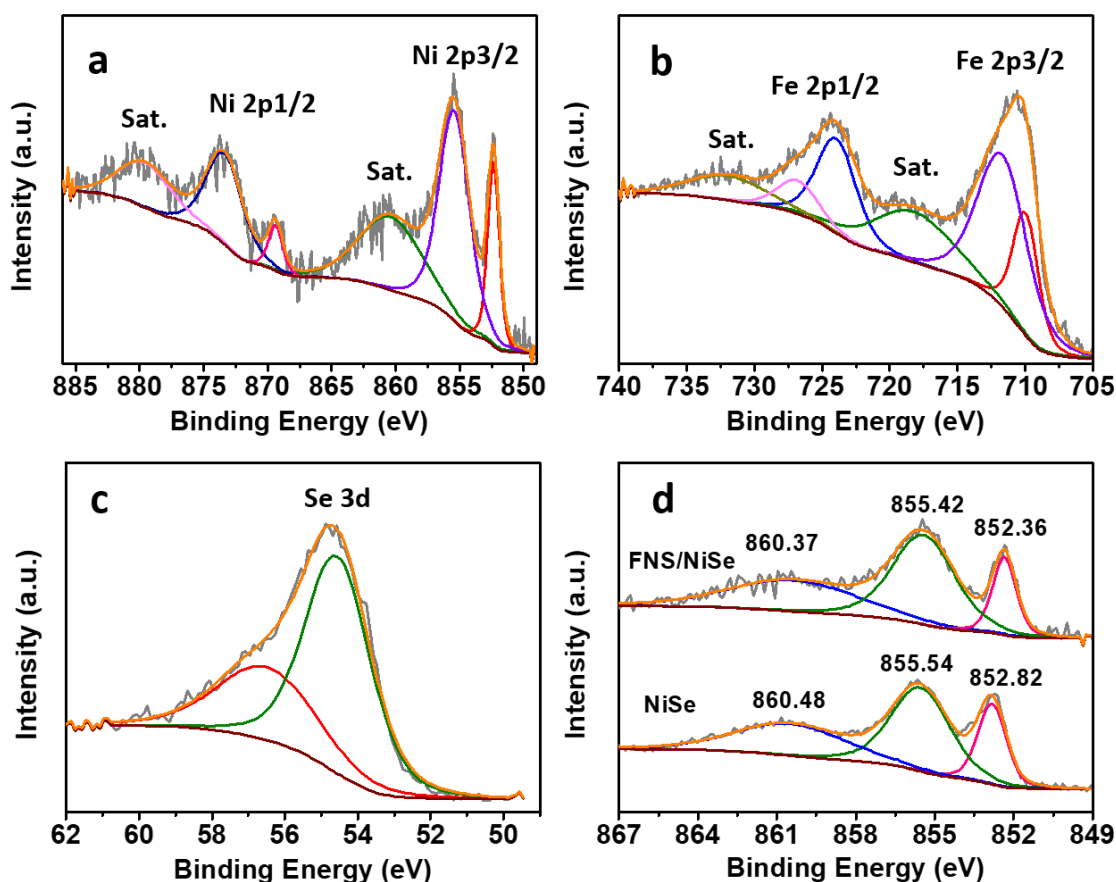


Fig. 3. XPS spectra of the as-synthesized FNS/NiSe foam for (a) Ni 2p, (b) Fe 2p and (c) Se 3d. (d) Regions and comparison of FNS/NiSe foam and NiSe foam in Ni section.

3.2. Electrocatalytic OER activity and stability

The electrocatalytic OER activities of the obtained samples were investigated in 1.0 M KOH at a scan rate of 1 mV s⁻¹ to minimize the capacitive current. The samples were directly applied as the working electrode, which avoids the use of binders so as to promote the efficient electron

transfer [31]. For comparison, blank Ni foam, blank FeNi alloy foam, NiSe foam and FNS foam were also studied under the same conditions. Fig. 4a shows the LSV curves with IR compensation [32]. As illustrated, the as-synthesized FNS/NiSe foam exhibits the significantly superior OER activity with an overpotential of only 242 mV to achieve 100 mA cm^{-2} , which is 54 and 98 mV less than that of the FNS foam and NiSe foam, respectively. An oxidation peak due to the reversible reaction of $\text{Ni}^{2+}/\text{Ni}^{3+}$ at around 1.41V (vs. RHE) before the onset of OER was observed in the NiSe foam, which was not obvious in the FNS/NiSe foam and FNS foam. The absence of oxidation peak is due to Fe suppression in the conversion of Ni^{2+} to Ni^{3+} , which has also been observed in other reports [29,33,34]. Notably, our FNS/NiSe foam compares favourably to most of the reported OER electrocatalysts in alkaline electrolyte (Table S1 in the Supporting Information). The OER kinetics of these five catalysts were estimated by calculating the Tafel slopes, which were derived from the LSV curves by plotting overpotential against $\log(J)$. As can be seen in Fig. 4b, the FNS/NiSe and FeNi foam both exhibit a Tafel slope of around 60 mV dec^{-1} , which is smaller than that of FNS foam (76 mV dec^{-1}) and NiSe foam ($130.4 \text{ mV dec}^{-1}$). This also indicates that the FNS/NiSe foam possesses a more favourable OER kinetics than the others, contributing to the enhanced catalytic performance. It is worth noting that catalysts that deliver high current density (e.g., 500 mA cm^{-2}) at low over potential (e.g., 300 mV) are highly desired for industrial applications [35,36]. In our work, the FNS/NiSe foam is able to reach a high current density of 500 mA cm^{-2} with an overpotential of merely 282 mV. The outstanding OER performance of the FNS/NiSe foam suggests that the $\text{Fe}_{4.4}\text{Ni}_{17.6}\text{Se}_{16}/\text{NiSe}$ hybrid foam is a promising candidate to replace the noble metal-based catalysts.

To estimate the amount of catalytically active sites, the ECSAs of the catalysts are evaluated by determining the C_{dl} [37,38]. CV curves under a series of scan rates in a certain potential range without redox process were collected and shown in Fig. S2 in the Supporting Information. Fig. 4c displays the corresponding plots of current difference vs scan rate of the catalysts. The results show that the FNS/NiSe foam has the largest C_{dl} value (4.92 mF cm^{-2}), which is several

times more than that of the FNS foam (2.57 mF cm^{-2}) and NiSe foam (1.63 mF cm^{-2}), indicating more exposure of catalytically active sites in FNS/NiSe foam. In order to understand the exact effect of the active sites in the OER process, we normalized the current densities to the corresponding ECSA, as presented in Fig. 4d. The current densities of FNS/NiSe foam are still much higher than those of the other four catalysts at the same overpotentials, which means that every catalytic site in FNS/NiSe foam is more active than that of FNS foam and NiSe foam. In addition, the electrochemical impedance spectroscopy (EIS) was further conducted to confirm the charge transport kinetics of the catalysts. The charge transfer resistances (R_{ct}) between the catalysts and the electrolyte were obtained by fitting the Nyquist plots with an equivalent circuit model, which fits the experimental data well (Fig. S3). EIS plots reveal that FNS/NiSe foam exhibits a much lower R_{ct} (1.226Ω) in comparison with that of FNS foam (5.71Ω) and NiSe foam (16.01Ω), suggesting that the FNS/NiSe foam exhibits much faster electron transfer kinetics during the OER [39].

The possible mechanisms of our FNS/NiSe foam for OER in the alkaline solution are proposed (See details in Fig. S4 in the Supporting Information) referring to the previous works [40-43]. In the oxygen evolution process, the formation of O-OH (step 3) is proposed as the rate-limiting step. The highly efficient OER performance of the FNS/NiSe foam is believed to come from the formation of the heterointerfaces. On one hand, the lower resistance of the FNS/NiSe foam comparing with the sole FNS or NiSe foam indicates that the low transfer resistance of FNS/NiSe foam is probably due to the construction of heterointerfaces. The low resistance can definitely improve the electron transfer in the OER process so as to help to lower the overpotential. On the other hand, the formation of the heterointerfaces can induce defects which are probably metal-rich according to the resistance data. These defects could help for adsorbing O and facilitating the formation of O-OH via nucleophilic attack, thus to promote these multielectron transfer steps during the OER activity. The contributions of heterointerfaces

1 and defects in the materials to the catalytic performance have been widely reported in the
2 previous work [44-49].

3 In addition to the catalytic activity, the long-time stability is also another important factor to
4 evaluate the OER performance. The as-obtained FNS/NiSe foam was tested at a constant
5 current density of 100 mA cm⁻² in 1.0 M KOH by chronopotentiometric measurement for 12 h.
6 Notably, the overpotential of the FNS/NiSe foam remained almost constant over 12 h
7 electrolysis, as shown in Fig. 4e. Besides, fig. 4f shows that the LSV curve after 1,000 CV
8 cycles is almost the same as the initial one, indicating its excellent stability. The accumulation
9 of bubbles on the surface of the catalysts can block the active sites of the catalysts or even
10 damage the structure of catalysts, which commonly appears among the bulk or solid materials.
11 We believe that the excellent stability, on the one hand, is due to the porous 3D structure of the
12 FNS/NiSe foam, which can release efficiently the O₂ bubbles generated during the
13 electrocatalytic reaction (Movie S1 in the Supporting Information). On the other hand, the high
14 crystallinity developed under the thermal selenization process can contribute to the good
15 stability as well [50,51]. The excellent stability was also observed in the FNS foam synthesized
16 via the same thermal selenization process (Fig. S5 in the Supporting Information). The
17 FNS/NiSe foam after the stability test over 12 h preserved the plate-like morphology as
18 indicated by the SEM image (Fig. S6 in the Supporting Information), which shows good
19 structure stability of the as-synthesized FNS/NiSe foam. Moreover, the crystal and electronic
20 structures of the FNS/NiSe foam also retained after electrolysis, which was further confirmed
21 by XRD and XPS characterization (Fig. S7 in the Supporting Information). All of the above
22 information provides strong evidences that the as-synthesized FNS/NiSe foam processes
23 excellent stability during the OER catalysis.

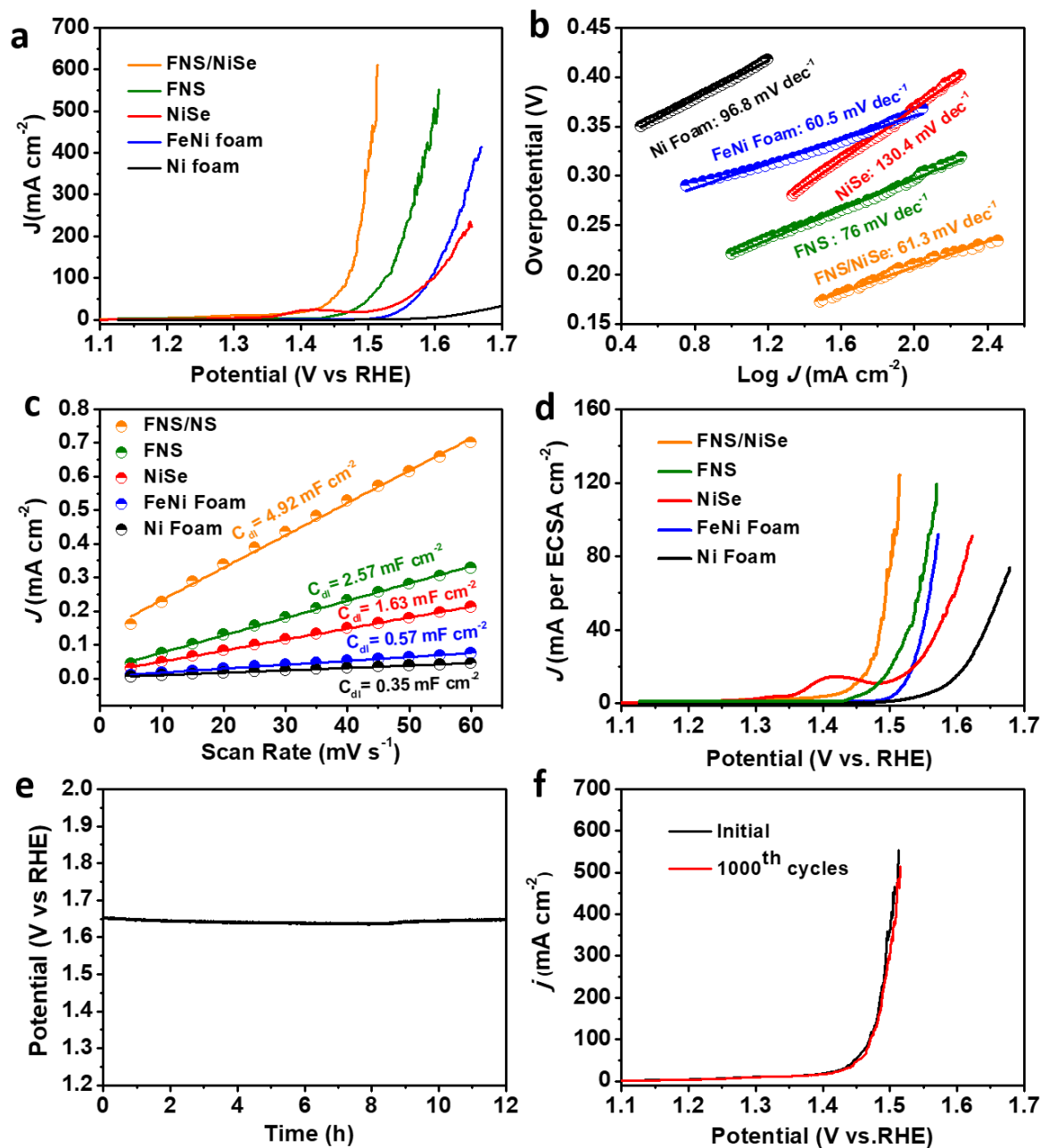


Fig. 4. (a) iR-corrected LSV curves of FNS/NiSe, FNS, NiSe, FeNi and Ni foam in 1.0 M KOH at a scan rate of 1 mV s⁻¹. (b) The corresponding Tafel plots. (c) The plot of charge current density differences vs scan rates. (d) ECSA-normalized polarization curves. (e) Chronopotentiometric curve of the FNS/NiSe foam (without iR correction) at a constant current density of 100 mA cm⁻² over a period of 12 h. (f) LSV curves for FNS/NiSe foam before and after 1000 CV cycles of stability test.

4. Conclusions

In summary, we have developed a simple method for direct synthesis of Fe_{4.4}Ni_{17.6}Se₁₆/NiSe hybrid foam via thermal selenization of the FeNi alloy foam as self-supported OER electrode. The FNS/NiSe foam displays remarkable OER activity in alkaline solution with an overpotential of only 242 mV to deliver a current density of 100 mA cm⁻², which is also feasible to reach a high current density of 500 mA cm⁻² at an overpotential of merely 282 mV. The direct utilization of FeNi alloy foam as precursor avoids complicated receipt and provides 3D porous structure to promote O₂ bubbles release and high surface area. The heterointerfaces and electron interactions in the FNS/NiSe foam contribute to highly-exposed active sites and efficient electron conductivity to further enhance OER performance. Meanwhile, this FNS/NiSe foam also exhibits impressive stability during the OER process, maintaining a current density of 100 mA cm⁻² for at least 12 h. Therefore, our work provides a simple strategy to fabricate hybrid transition metal chalcogenides as low-cost, efficient and durable electrodes for OER.

Acknowledgements

This work is financially supported by the National Natural Science Foundation of China (No. 61575167) and Shenzhen Science and Technology Innovation Commission (Project No.: JCYJ20170303160136888).

References

- [1] T.R. Cook, D.K. Dogutan, S.Y. Reece, Y. Surendranath, T.S. Teets, D.G. Nocera, Solar energy supply and storage for the legacy and nonlegacy worlds, *Chem. Rev.* 110 (2010) 6474-6502.
- [2] E.E. Benson, C.P. Kubiak, A.J. Sathrum, J.M. Smieja, Electrocatalytic and homogeneous approaches to conversion of CO₂ to liquid fuels, *Chem. Soc. Rev.* 38 (2009) 89-99.
- [3] J.A. Turner, Sustainable hydrogen production, *Science* 305 (2004) 972.
- [4] M.W. Kanan, D.G. Nocera, In situ formation of an oxygen-evolving catalyst in neutral water containing phosphate and Co²⁺, *Science* 321 (2008) 1072.
- [5] M.T.M. Koper, Thermodynamic theory of multi-electron transfer reactions: implications for electrocatalysis, *J. Electroanal. Chem.* 660 (2011) 254-260.
- [6] T. Kinoshita, J.-i. Fujisawa, J. Nakazaki, S. Uchida, T. Kubo, H. Segawa, Enhancement of near-IR photoelectric conversion in dye-sensitized solar cells using an osmium sensitizer with strong spin-forbidden transition, *J. Phys. Chem. Lett.* 3 (2012) 394-398.

- [7] M.S. Burke, S. Zou, L.J. Enman, J.E. Kellon, C.A. Gabor, E. Pledger, S.W. Boettcher, Revised oxygen evolution reaction activity trends for first-row transition-metal (Oxy)hydroxides in alkaline media, *J. Phys. Chem. Lett.* 6 (2015) 3737-3742.
- [8] J.R. Galán-Mascarós, Water oxidation at electrodes modified with earth-abundant transition-metal catalysts, *Chemelectrochem* 2 (2015) 37-50.
- [9] A. Singh, L. Spiccia, Water oxidation catalysts based on abundant 1st row transition metals, *Coord. Chem. Rev.* 257 (2013) 2607-2622.
- [10] X. Han, X. Tong, G. Wu, N. Yang, X.-Y. Guo, Carbon fibers supported NiSe nanowire arrays as efficient and flexible electrocatalysts for the oxygen evolution reaction, *Carbon* 129 (2018) 245-251.
- [11] Z. Pu, Y. Luo, A.M. Asiri, X. Sun, Efficient electrochemical water splitting catalyzed by electrodeposited nickel diselenide nanoparticles based film, *ACS Appl. Mater. Interfaces* 8 (2016) 4718-4723.
- [12] A. Sivanantham, S. Shanmugam, Nickel selenide supported on nickel foam as an efficient and durable non-precious electrocatalyst for the alkaline water electrolysis, *Appl. Catal., B* 203 (2017) 485-493.
- [13] A.T. Swesi, J. Masud, M. Nath, Nickel selenide as a high-efficiency catalyst for oxygen evolution reaction, *Energy Environ. Sci.* 9 (2016) 1771-1782.
- [14] C. Tang, N. Cheng, Z. Pu, W. Xing, X. Sun, NiSe nanowire film supported on nickel foam: an efficient and stable 3D bifunctional electrode for full water splitting, *Angew. Chem., Int. Ed.* 127 (2015) 9483-9487.
- [15] Z. Gao, J. Qi, M. Chen, W. Zhang, R. Cao, An electrodeposited NiSe for electrocatalytic hydrogen and oxygen evolution reactions in alkaline solution, *Electrochim. Acta* 224 (2017) 412-418.
- [16] M.F. Kibria, M.S. Mridha, Electrochemical studies of the nickel electrode for the oxygen evolution reaction, *Int. J. Hydrogen Energy* 21 (1996) 179-182.
- [17] J.-X. Feng, S.-H. Ye, H. Xu, Y.-X. Tong, G.-R. Li, Design and synthesis of FeOOH/CeO₂ heterolayered nanotube electrocatalysts for the oxygen evolution reaction, *Adv. Mater.* 28 (2016) 4698-4703.
- [18] F. Ming, H. Liang, H. Shi, G. Mei, X. Xu, Z. Wang, Hierarchical (Ni,Co)Se₂/carbon hollow rhombic dodecahedra derived from metal-organic frameworks for efficient water-splitting electrocatalysis, *Electrochim. Acta* 250 (2017) 167-173.
- [19] J.-X. Feng, H. Xu, Y.-T. Dong, S.-H. Ye, Y.-X. Tong, G.-R. Li, FeOOH/Co/FeOOH hybrid nanotube arrays as high-performance electrocatalysts for the oxygen evolution reaction, *Angew. Chem. Int., Ed.* 55 (2016) 3694-3698.
- [20] H. Liang, A.N. Gandi, C. Xia, M.N. Hedhili, D.H. Anjum, U. Schwingenschlögl, H.N. Alshareef, Amorphous NiFe-OH/NiFeP electrocatalyst fabricated at low temperature for water oxidation applications, *ACS Energy Lett.* 2 (2017) 1035-1042.
- [21] B. Xu, H. Yang, L. Yuan, Y. Sun, Z. Chen, C. Li, Direct selenylation of mixed Ni/Fe metal-organic frameworks to NiFe-Se/C nanorods for overall water splitting, *J. Power Sources* 366 (2017) 193-199.
- [22] F. Zhang, Y. Pei, Y. Ge, H. Chu, S. Craig, P. Dong, J. Cao, P.M. Ajayan, M. Ye, J. Shen, Controlled synthesis of eutectic NiSe/Ni₃Se₂ self-supported on Ni Foam: an excellent bifunctional electrocatalyst for overall water splitting, *Adv. Mater. Interfaces* 5 (2018) 1701507.
- [23] H. Zhou, F. Yu, Y. Liu, J. Sun, Z. Zhu, R. He, J. Bao, W.A. Goddard, S. Chen, Z. Ren, Outstanding hydrogen evolution reaction catalyzed by porous nickel diselenide electrocatalysts, *Energy Environ. Sci.* 10 (2017) 1487-1492.
- [24] X. Lu, C. Zhao, Electrodeposition of hierarchically structured three-dimensional nickel-iron electrodes for efficient oxygen evolution at high current densities, *Nat. Commun.* 6 (2015) 6616.

- [25] S. Saha, A.K. Ganguli, FeCoNi alloy as noble metal-free electrocatalyst for oxygen evolution reaction (OER), *ChemistrySelect* 2 (2017) 1630-1636.
- [26] Y. Ma, X. Dai, M. Liu, J. Yong, H. Qiao, A. Jin, Z. Li, X. Huang, H. Wang, X. Zhang, Strongly coupled FeNi alloys/NiFe₂O₄@carbonitride layers-assembled microboxes for enhanced oxygen evolution reaction, *ACS Appl. Mater. Interfaces* 8 (2016) 34396-34404.
- [27] A. Sivanantham, P. Ganesan, S. Shanmugam, Hierarchical NiCo₂S₄ nanowire arrays supported on Ni foam: an efficient and durable bifunctional electrocatalyst for oxygen and hydrogen evolution reactions, *Adv. Funct. Mater.* 26 (2016) 4661-4672.
- [28] Y. Du, G. Cheng, W. Luo, Colloidal synthesis of urchin-like Fe doped NiSe₂ for efficient oxygen evolution, *Nanoscale* 9 (2017) 6821-6825.
- [29] Z. Wang, J. Li, X. Tian, X. Wang, Y. Yu, K.A. Owusu, L. He, L. Mai, Porous nickel-iron selenide nanosheets as highly efficient electrocatalysts for oxygen evolution reaction, *ACS Appl. Mater. Interfaces* 8 (2016) 19386-19392.
- [30] J. Nai, Y. Lu, L. Yu, X. Wang, X.W. Lou, Formation of Ni-Fe mixed diselenide nanocages as a superior oxygen evolution electrocatalyst, *Adv. Mater.* 29 (2017) 1703870.
- [31] C.-Z. Yuan, Z.-T. Sun, Y.-F. Jiang, Z.-K. Yang, N. Jiang, Z.-W. Zhao, U.Y. Qazi, W.-H. Zhang, A.-W. Xu, One-step in situ growth of iron-nickel sulfide nanosheets on FeNi alloy foils: high-performance and self-supported electrodes for water oxidation, *Small* 13 (2017) 1604161.
- [32] Z. Xing, Q. Liu, A.M. Asiri, X. Sun, Closely interconnected network of molybdenum phosphide nanoparticles: a highly efficient electrocatalyst for generating hydrogen from water, *Adv. Mater.* 26 (2014) 5702-5707.
- [33] Z. Lu, W. Xu, W. Zhu, Q. Yang, X. Lei, J. Liu, Y. Li, X. Sun, X. Duan, Three-dimensional NiFe layered double hydroxide film for high-efficiency oxygen evolution reaction, *Chem. Commun.* 50 (2014) 6479-6482.
- [34] K. Fominykh, P. Chernev, I. Zaharieva, J. Sicklinger, G. Stefanic, M. Döblinger, A. Müller, A. Pokharel, S. Böcklein, C. Scheu, T. Bein, D. Fattakhova-Rohlfing, Iron-doped nickel oxide nanocrystals as highly efficient electrocatalysts for alkaline water splitting, *ACS Nano* 9 (2015) 5180-5188.
- [35] Y. Li, C. Zhao, Iron-doped nickel phosphate as synergistic electrocatalyst for water oxidation, *Chem. Mater.* 28 (2016) 5659-5666.
- [36] H. Zhou, F. Yu, J. Sun, R. He, S. Chen, C.-W. Chu, Z. Ren, Highly active catalyst derived from a 3D foam of Fe(PO₃)₂/Ni₂P for extremely efficient water oxidation, *Proc. Natl. Acad. Sci. U.S.A* 114 (2017) 5607-5611.
- [37] M.A. Lukowski, A.S. Daniel, F. Meng, A. Forticaux, L. Li, S. Jin, enhanced hydrogen evolution catalysis from chemically exfoliated metallic MoS₂ nanosheets, *J. Am. Chem. Soc.* 135 (2013) 10274-10277.
- [38] F. Song, X. Hu, Ultrathin cobalt-manganese layered double hydroxide is an efficient oxygen evolution catalyst, *J. Am. Chem. Soc.* 136 (2014) 16481-16484.
- [39] T. Wang, L. Liu, Z. Zhu, P. Papakonstantinou, J. Hu, H. Liu, M. Li, Enhanced electrocatalytic activity for hydrogen evolution reaction from self-assembled monodispersed molybdenum sulfide nanoparticles on an Au electrode, *Energy Environ. Sci.* 6 (2013) 625-633.
- [40] N.-T. Suen, S.-F. Hung, Q. Quan, N. Zhang, Y.-J. Xu, H.M. Chen, Electrocatalysis for the oxygen evolution reaction: recent development and future perspectives, *Chem. Soc. Rev.* 46 (2017) 337-365.
- [41] M.-R. Gao, Y.-F. Xu, J. Jiang, Y.-R. Zheng, S.-H. Yu, Water oxidation electrocatalyzed by an efficient Mn₃O₄/CoSe₂ nanocomposite, *J. Am. Chem. Soc.* 134 (2012) 2930-2933.
- [42] H. Zhu, R. Jiang, X. Chen, Y. Chen, L. Wang, 3D nickel-cobalt diselenide nanonetwork for highly efficient oxygen evolution, *Sci. Bull.* 62 (2017) 1373-1379.
- [43] B.S. Yeo, A.T. Bell, Enhanced activity of gold-supported cobalt oxide for the electrochemical evolution of oxygen, *J. Am. Chem. Soc.* 133 (2011) 5587-5593.

- 1 [44] G. Zhu, X. Xie, Y. Liu, X. Li, K. Xu, X. Shen, Y. Yao, S.A. Shah, Fe₃O₄@NiS_x/rGO
2 composites with amounts of heterointerfaces and enhanced electrocatalytic properties for
3 oxygen evolution, *Appl. Surf. Sci.* 442 (2018) 256-263.
- 4 [45] K. Kumar, C. Canaff, J. Rousseau, S. Arrii-Clacens, T.W. Napporn, A. Habrioux, K.B.
5 Kokoh, Effect of the oxide-carbon heterointerface on the activity of Co₃O₄/NRGO
6 nanocomposites toward ORR and OER, *J. Phys. Chem. C* 120 (2016) 7949-7958.
- 7 [46] Y. Yang, H. Fei, G. Ruan, C. Xiang, J.M. Tour, Efficient electrocatalytic oxygen evolution
8 on amorphous nickel-cobalt binary oxide nanoporous layers, *ACS Nano* 8 (2014) 9518-9523.
- 9 [47] T. Cheng, W. Hao-Fan, C. Xiang, L. Bo-Quan, H. Ting-Zheng, Z. Bingsen, Z. Qiang, T.
10 Maria-Magdalena, W. Fei, Topological defects in metal-free nanocarbon for oxygen
11 electrocatalysis, *Adv. Mater.* 28 (2016) 6845-6851.
- 12 [48] J. Chen, G. Wu, T. Wang, X. Li, M. Li, Y. Sang, H. Liu, Carrier step-by-step transport
13 initiated by precise defect distribution engineering for efficient photocatalytic hydrogen
14 generation, *ACS Appl. Mater. Inter.* 9 (2017) 4634-4642.
- 15 [49] F. Cheng, J. Shen, B. Peng, Y. Pan, Z. Tao, J. Chen, Rapid room-temperature synthesis of
16 nanocrystalline spinels as oxygen reduction and evolution electrocatalysts, *Nat. Chem.* 3 (2010)
17 79.
- 18 [50] R.D.L. Smith, M.S. Prévot, R.D. Fagan, Z. Zhang, P.A. Sedach, M.K.J. Siu, S. Trudel, C.P.
19 Berlinguette, Photochemical route for accessing amorphous metal oxide materials for water
20 oxidation catalysis, *Science* 340 (2013) 60.
- 21 [51] M. Gong, H. Dai, A mini review of NiFe-based materials as highly active oxygen evolution
22 reaction electrocatalysts, *Nano Res.* 8 (2015) 23-39.

23
24